Supplemental Materials: Self-assembly and rheology of dipolar colloids in simple shear - studied by multi-particle collision dynamics

1 Simulation parameters

The choice of the simulation parameters preserves the hierarchy of the physical and simulation timescales as described previously[S1,S2] to ensure consistency with typical colloidal systems: the ratio of the mass of the colloid M_p to the mass of the MPCD particle m_f is 79, the nominal number of the MPCD particles per bin is $\langle n_J \rangle = 6$. The extent of the collision environment a defines the spatial accuracy of the hydrodynamic flow[S2] and is set to $a = 0.5\sigma$ to properly resolve the flow on the scale of the aggregates $n \geq 2$, whose contribution to the viscosity scales as $\propto n^3$. The mean free path of the MPCD particles is $l_{mpcd} = \Delta t_{mpcd} \left(\sqrt{\beta m_f}\right)^{-1} = 0.3\sigma$ ensuring Galilean invariance[S1,S3]. The time between the multi-particle collisions is $\Delta t_{mpcd} = 0.034\tilde{t}$, where $\tilde{t} = \sigma\sqrt{\beta M_p}$. The simulations are performed with LAMMPS[S4,S5] in a rheometric slit channel of extent L_x, L_y, L_z (volume $V = L_x L_y L_z$). For zero-field simulations $L_x = L_y = L_z = 24\sigma$, whereas, for simulations with an applied field (in y direction) the size of the box is increased for larger interaction parameters λ: $L_x = L_z = 16\sigma$ ($\lambda < 4$) or 24σ ($\lambda \geq 4$) and $L_y = 32\sigma$ ($\lambda < 4$), 48σ ($\lambda = 4$), 72σ ($\lambda \geq 5$) to accommodate the growing microstructure. Periodic BCs are used in the x (flow) and z (vorticity) directions, in the y (gradient) direction the channel is bounded by the free-slip walls realizing reflections $v_n \rightarrow -v_n$ of the incoming MPCD particles and a short-range repulsive potential of the form (4) (Main text) is applied to the approaching colloids to prevent percolation of the microstructure at larger λ. The colloids are randomly dispersed at a predefined volume fraction ϕ (in all simulations $\phi = 5vol.\%$ except when ϕ itself is varied) with the total number $N_p = \phi v_p^{-1} V$, where $V = L_x L_y L_z$ is the volume of the simulation box and $v_p = \frac{1}{6}\pi\sigma^3$ is the volume of a colloidal particle. The total number of the MPCD particles is $N_{mpcd} = a^{-3} V (1-\phi) \langle n_J \rangle$. In the flow simulations the shearing is induced by adjusting the streaming velocities $\langle \boldsymbol{v} \rangle_J$ of the MPCD particles in the bins nearest to the channel walls. After a brief limit run the system was equilibrated for $t_{eq} = 4{,}000\tilde{t}$ ($\lambda < 4$), $8{,}000\tilde{t}$ ($\lambda = 4$) or $20{,}000\tilde{t}$ ($\lambda \geq 5$) followed by a production run of $4{,}000 - 20{,}000\tilde{t}$, depending on the size of the system and the shear rate. Bin-wise sampling was used to measure the flow profile and determine the actual shear rate $\dot{\gamma}$. Every simulation was repeated between 4 and 32 times to produce statistically independent trajectories and reduce scatter in the measured observables. The error is reported in terms of the standard deviation.

2 Equilibrium partition function

Accounting for just the nearest neighbor interactions the partition function of a self-assembled chain is[S6]

$$Z_n = \int e^{-\beta \sum_{i=1}^{n-1} U_{dd}(\boldsymbol{\mu_i}, \boldsymbol{\mu}_{i+1}, \boldsymbol{r}_{i,i+1}) + U_{ss}(r_{i,i+1})} \prod_{i=1}^{n} \frac{\boldsymbol{d\mu_i}}{4\pi} \prod_{i=1}^{n-1} \boldsymbol{dr}_{i,i+1} \tag{S1}$$

whereas the interactions beyond the directly adjacent particles along the chain lead to the renormalization of the bond strength $\lambda \rightarrow \lambda\zeta(3), \zeta(3) = 1.202$.[S7,S8] The pair partition function Z_2 in zero and infinite field[S8]

$$H \rightarrow 0 : Z_2(0) = 8\lambda \int_{0.5}^{\lambda} \frac{dl}{l^3} \int_0^1 dx \frac{\sinh\left(l\frac{1-3x^2}{2}\right)}{1-3x^2} I_0\left(3l\frac{1-x^2}{2}\right) \tag{S2}$$

$$H \rightarrow \infty : Z_2(\infty) = 4\lambda \int_{0.5}^{\lambda} \frac{dl}{l^2} \int_0^1 dx e^{l\left(3x^2-1\right)} \tag{S3}$$

3 Chain deviation angle

Tallying the dipolar ($\boldsymbol{F^m}$) and hydrodynamic ($\boldsymbol{F^h}$) force couples starting from the center ($i = 1$) of the chain[S11,S12] in Fig. S1: $\boldsymbol{\Gamma}^{m,h} = 2\sum_{i=1}^{\nu_n} i\sigma \boldsymbol{e}_r \times \boldsymbol{F}_i^{m,h}$ where $\boldsymbol{e}_r$ is the director vector of the chain and $\nu_n = \frac{n-1}{2}$. The energy of the magnetic bond $U_{dd}(\boldsymbol{e}_y, \boldsymbol{e}_y, \boldsymbol{e}_r) = -\lambda kT\left(3\cos^2\theta_n - 1\right)$ ($\boldsymbol{e}_y$ is the unit vector in the vertical (y) direction) produces a magnetic force couple: $\boldsymbol{F}_\theta^m = -\frac{1}{\sigma}\frac{\partial U_{dd}}{\partial\theta}\boldsymbol{e}_\theta = -6\lambda kT\sigma^{-1}\cos\theta_n \sin\theta_n \boldsymbol{e}_\theta$ and $-\boldsymbol{F}_\theta^m$ acting on the i$^{\text{th}}$ and (i-1)$^{\text{th}}$ particles ($\boldsymbol{e}_\theta$ is the unit vector in the direction of increasing deviation angle θ_n). Summing the individual contributions along the chain, a realigning torque is provided by the end particles, where the magnetic force couples are not compensated $\boldsymbol{\Gamma}^m = -6(n-1)\lambda kT\cos\theta_n \sin\theta_n \boldsymbol{e}_r \times \boldsymbol{e}_\theta$. In turn, assuming the free draining limit, the hydrodynamic force acting on the i$^{\text{th}}$ particle of the n-particle chain in simple shear $\boldsymbol{F}_i^h = 6\pi\eta_0\sigma^2 i\dot{\gamma}\cos\theta_n \boldsymbol{e}_x$ ($\boldsymbol{e}_x$ is the unit vector in the x direction, η_0 is the vicosity of the solvent) and the deviating torque $\boldsymbol{\Gamma}^h = \frac{1}{2}n\left(n^2-1\right)\pi\eta_0\dot{\gamma}\sigma^3\cos^2\theta_n \boldsymbol{e}_r \times \boldsymbol{e}_\theta$. The torque equilibrium $\boldsymbol{\Gamma^m} + \boldsymbol{\Gamma^h} = 0$ yields the deviation angle θ_n of the n-mer

$$\tan\theta_n = \frac{1}{12}\left(n^2+n\right)Mn \tag{S4}$$

4 Critical chain length

Considering the radial force balance of a rigid chain[S11,S12] (Fig. S1): the n-particle chain is broken, when the strength of the bond $F_r^m = -\frac{\partial U_{dd}}{\partial r} = -3\lambda kT\sigma^{-1}\left(3\cos^2\theta_n - 1\right)$ is overcome by the overall shear force extending the chain $F_r^h = \sum_{i=1}^{\nu_n} \boldsymbol{F}_i^h \cdot \boldsymbol{e}_r = \frac{3}{4}\left(n^2-1\right)\pi\eta_0\dot{\gamma}\sigma^2\cos\theta_n \sin\theta_n$. The equation for the maximum length of a stable chain is produced from the radial mechanical balance of the bonding force versus the hydrodynamic erosive force $F_r^m + F_r^h = 0$ accounting for eq. (S4): $4n^4 + 5n^3 - 2n^2 - 3n - \frac{288}{Mn^2} = 0$. To a leading order in n the critical length is

$$n_{crit} \approx \sqrt{\frac{6\sqrt{2}}{Mn}} \tag{S5}$$

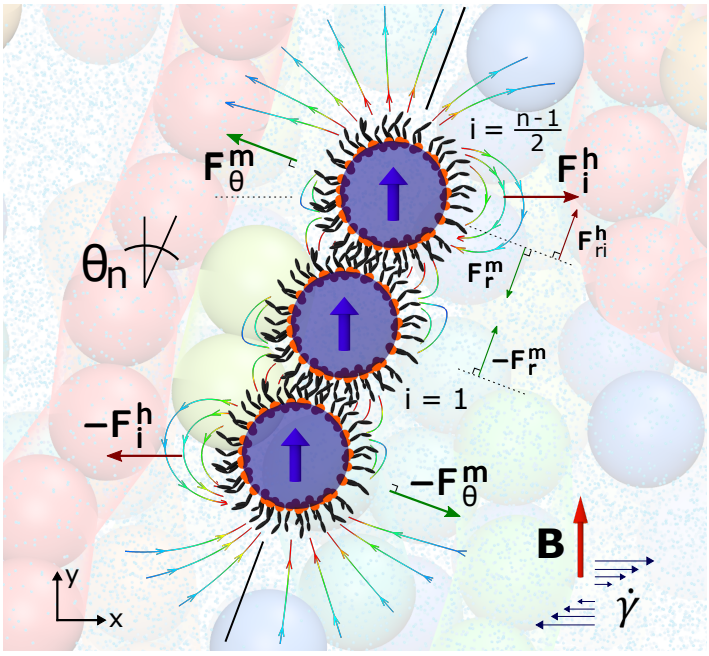

Figure S1 Schematic representation of a straight chain of dipolar particles (here a trimer containing $n = 3$ particles) with field-aligned dipoles and acting forces in simple shear and strong magnetic field applied vertically, magnetic field lines around the chain (note: vector lengths not to scale). The particles are indexed from the center ($i = 1$). The peaks of the positional probability distribution P_3 along the director show that the central particle is well localized near the center of mass, whereas the end particles are less confined.

5 Geometrical coefficients of an n-particle chain

The geometrical coefficients used in eq. (26) are[S9–S11]

$$\alpha_n = \frac{1}{n\alpha_0'}, \quad \beta_n = \frac{2\left(n^2-1\right)}{n\left(n^2\alpha_0+\beta_0\right)}, \quad \xi_n = \frac{4}{\left(n^2+1\right)n\beta_0'} - \frac{2}{n\alpha_0'} \tag{S6}$$

$$\lambda_n = \frac{n^2-1}{n^2+1}, \quad \chi_n = \frac{2\alpha_0''}{n\alpha_0'\beta_0''} - \frac{8}{n\left(n^2+1\right)\beta_0'} + \frac{2}{n\alpha_0'} \tag{S7}$$

where the elliptic integrals for the case of an ellipsoid of revolution are

$$\alpha_0 = \int_0^\infty \frac{ds}{\left(n^2+s\right)Q_n(s)}, \quad \beta_0 = \int_0^\infty \frac{ds}{\left(1+s\right)Q_n(s)} \tag{S8}$$

$$\alpha_0' = \int_0^\infty \frac{ds}{\left(1+s\right)^2 Q_n(s)}, \quad \beta_0' = \int_0^\infty \frac{ds}{\left(n^2+s\right)\left(1+s\right)Q_n(s)} \tag{S9}$$

$$\alpha_0'' = \int_0^\infty \frac{sds}{\left(1+s\right)^2 Q_n(s)}, \quad \beta_0'' = \int_0^\infty \frac{sds}{\left(n^2+s\right)\left(1+s\right)Q_n(s)} \tag{S10}$$

with $Q_n(s) = (1+s)\sqrt{n^2+s}$.

References

[S1] M. Hecht, J. Harting, T. Ihle, H. J. Herrmann, Phys. Rev. E **72**, 011408 (2005).

[S2] J. T. Padding, A. A. Louis, Phys. Rev. E **74**, 031402 (2006).

[S3] T. Ihle, E. Tuzel, D. M. Kroll, Phys. Rev. E **70**, 035701 (2004).

[S4] S. Plimpton, J. Comput. Phys. **117**, 1-19 (1995).

[S5] M. K. Petersen, J. B. Lechman, S. J. Plimpton, G. S. Grest, P. J. in 't Veld, P. R. Schunk, J. Chem. Phys. **132**, 174106 (2010).

[S6] M. A. Osipov, P. I. C. Teixeira, M. M. Telo da Gama, J. Phys. Condens. Matter **16**, 2597-2609 (1996).

[S7] P. C. Jordan, Mol. Phys. **25**, 961-973 (1973).

[S8] K. I. Morozov, M. I. Shliomis, J. Phys. Condens. Matter **16**, 3807-3818 (2004).

[S9] V. N. Pokrovskii, Sov. Phys. Uspekhi **14**, 737-746 (1972).

[S10] A. Yu. Zubarev, L. Yu. Iskakova, Phys. Rev. E **61**, 5415-5421 (2000).

[S11] A. Yu. Zubarev, L. Yu. Iskakova, Physica A **382**, 378-388 (2007).

[S12] J. E. Martin, R. A. Anderson, J. Chem. Phys. **104**, 4814-4827 (1996).

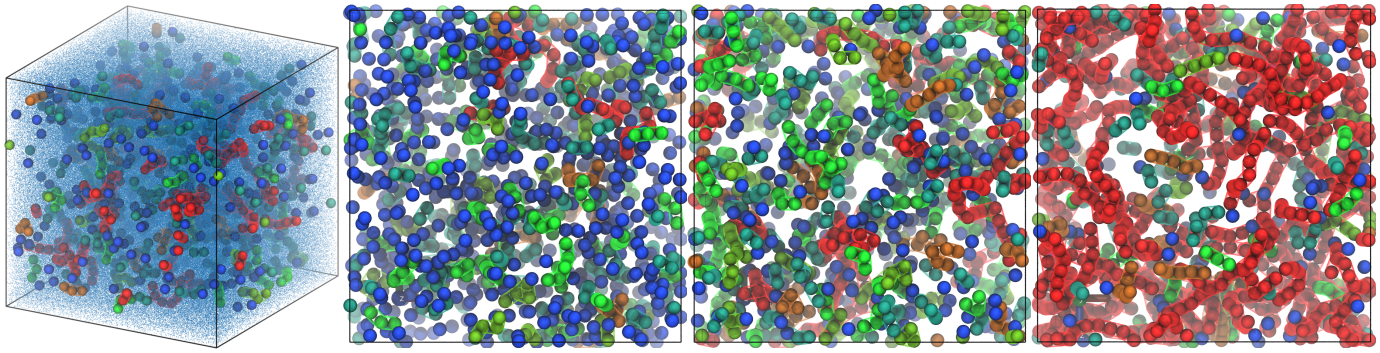

Figure S2 *(a)* - simulation snapshot (box size $24\sigma \times 24\sigma \times 24\sigma$) of spontaneous association of dipolar particles without an applied field at a volume fraction $\phi = 5\%$ and dipole interaction parameter $\lambda = 4$. Blue background depicts a sea of MPCD point particles representing the solvent. Simulation snapshots for varying strength of dipolar interactions: *(b)* $\lambda = 3$, *(c)* $\lambda = 4$, *(d)* $\lambda = 5$. Substantial lengthening and branching of the particle chains is observed at larger λ. Particles color-coded by chain length n: monomers ($n = 1$) are blue, $n \geq 10$ - red.

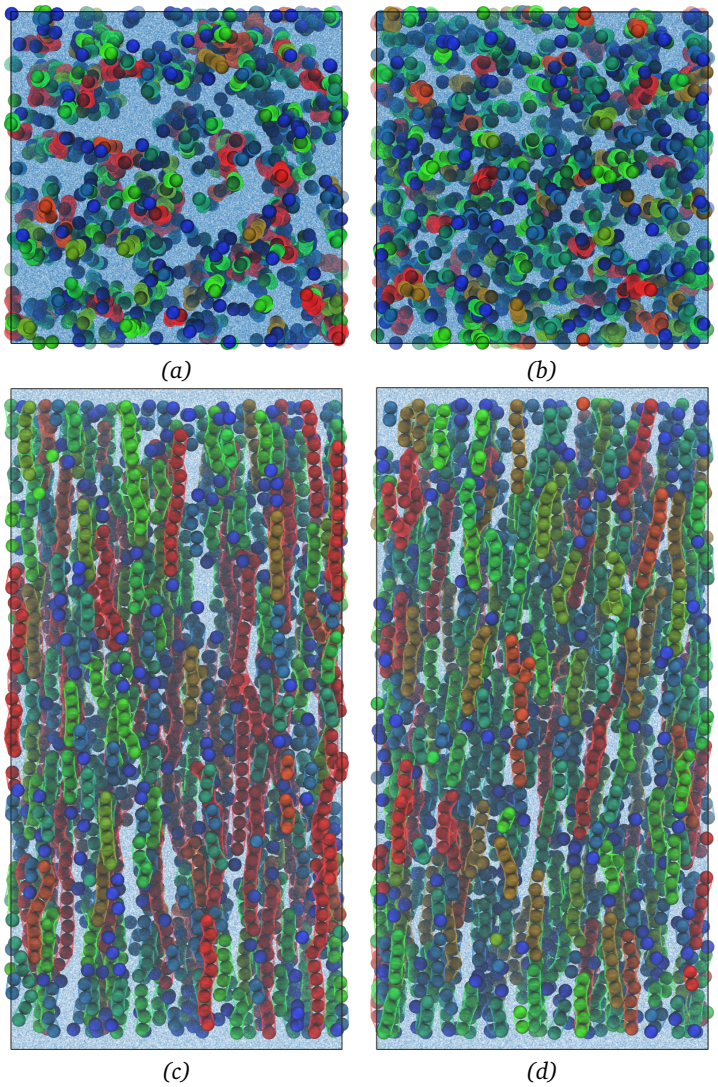

Figure S3 Simulation snapshots (box size $24\sigma \times 48\sigma \times 24\sigma$) with strong vertical external field at a volume fraction $\phi = 5\%$ and dipole interaction parameter $\lambda = 4$ in equilibrium (left - (a), (c)) and under shear (right - (b), (d)) show chains of various length aligned in the direction of the field and deviated by imposed shear flow at $Mn \approx 0.012$. Side view - (c), (d) along the vorticity direction. Top view - (a), (b) along the direction of the applied field showing that the chains are uniformly dispersed within the layer in either case. Particles color-coded by chain length n: monomers ($n = 1$) are blue, $n \geq 10$ - red.

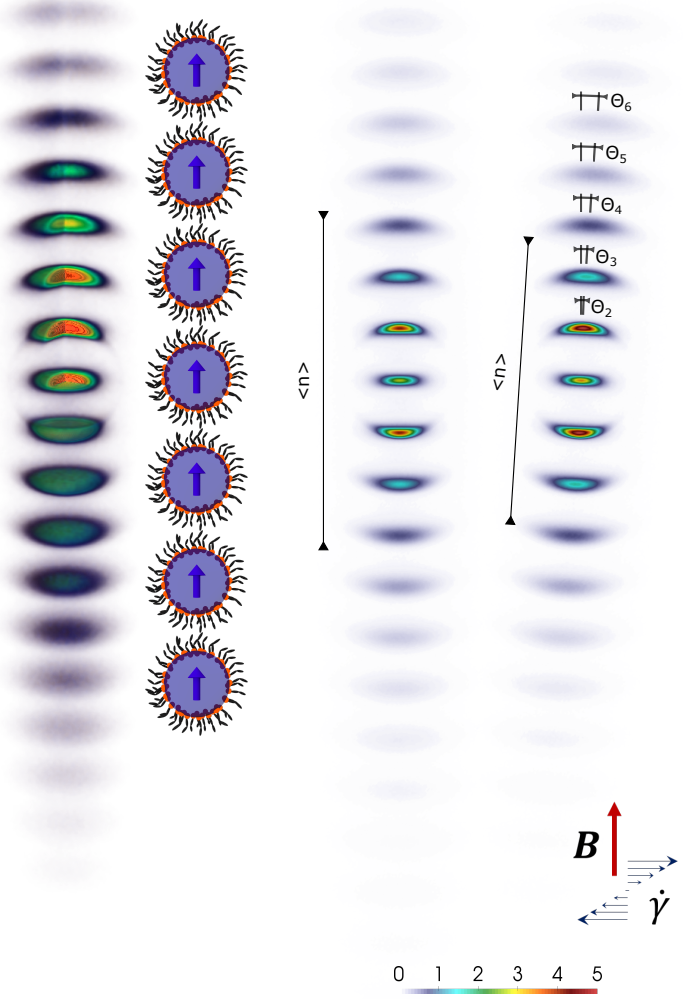

Figure S4 Calculated positional probability density distribution functions $P(\boldsymbol{r})$ corresponding to the simulations in Figure S3 ($\lambda = 4$, $\phi = 5\%$, note: free-floating monomer contributions are substracted). Left - 3D PDF $P(\boldsymbol{r})$ in equilibrium. Right - projection of the PDF $P(x,y) = \int P(\boldsymbol{r})\,dz$ onto the shear (velocity-vorticity) plane for the same system in equilibrium and at a shear rate $Mn \approx 0.012$. The deviation of the n–particle chains by the angle θ_n from the direction of the field is visible in the PDF. The bars show the average chain length $\langle n \rangle$ for comparison.

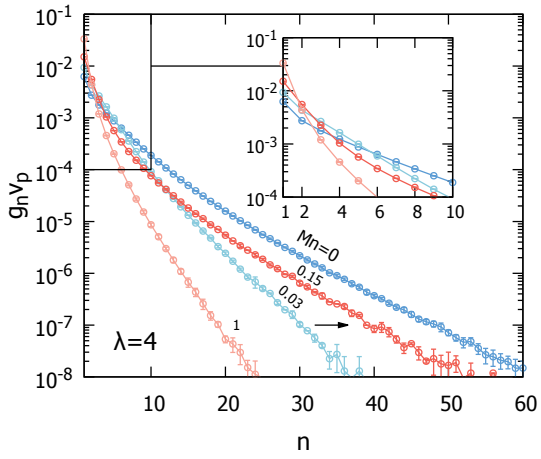

Figure S5 Chain length distributions g_n in simple shear (with reduced shear rate Mn) and strong external field for $\phi = 5\%$ and $\lambda = 4$; $v_p = \frac{1}{6}\pi\sigma^3$ is the particle volume. The inset shows a detailed view of the initial region. The recovery of the tail of the chain length distribution is observed at approx. $0.03 < Mn < 0.15$ signifying a transition into a shear-banded state.

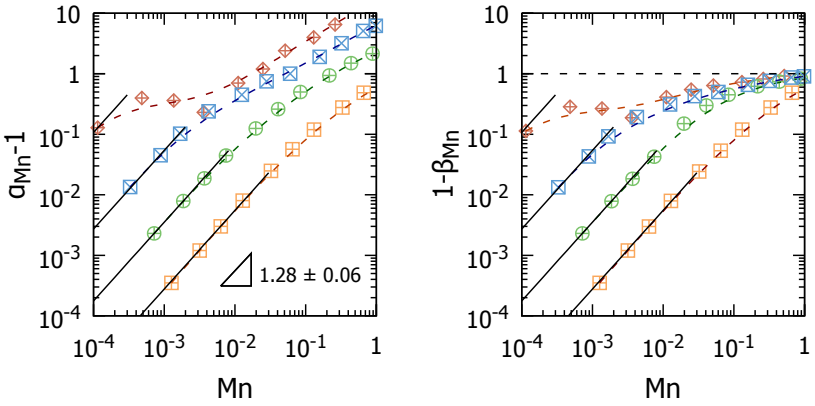

Figure S6 Scaling factors α_{Mn} and β_{Mn} used to collapse the non-equilibrium simulation data in Figure 6 (Main text) as a function of the Mason number Mn for $\lambda = 2$ (⊞), $\lambda = 3$ (⊕), $\lambda = 4$ (⊠), $\lambda = 5$ (⊕). For lower shear rates $Mn < 10^{-2}$ $\alpha_{Mn} \cdot \beta_{Mn} \approx 1$ and $\alpha_{Mn} - 1 \approx 1 - \beta_{Mn}$. The lines are intended to guide the eye.

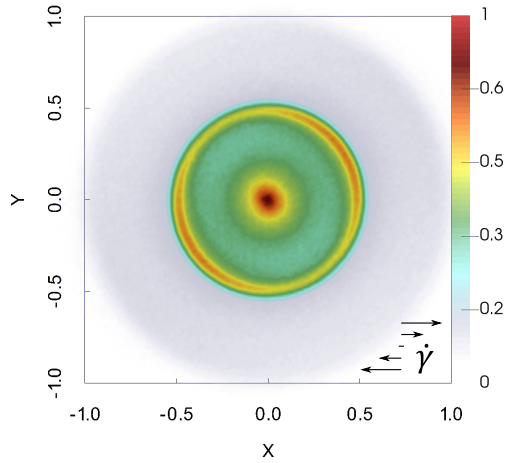

Figure S7 Projection of the non-equilibrium PDF $P(\boldsymbol{r})$ onto the shear (velocity-vorticity) plane without an applied field at a volume fraction $\phi = 5\%$, dipole interaction parameter $\lambda = 4$ and $Mn \approx 0.016$, showing the deformation of the conformations ellipsoid in simple shear.

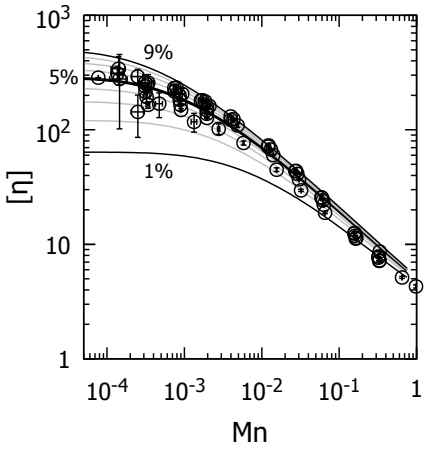

Figure S8 Intrinsic viscosity $[\eta]$ as a function of the Mason number Mn for varying fraction of dipolar particles $\phi = 1\% - 9\%$ at $\lambda = 4$. A series of calculations has been performed with varying volume fractions $\phi = 1\% - 9\%$ of the colloidal particles to check whether the intrinsic viscosity (28) provides an appropriate scaling for a self-assembled system, where the contributions of the individual colloidal particles should not be additive. The figure shows that for all considered volume fractions the shear thinning regions satisfactorily collapse onto a single curve, which is supported by the chain model. In turn, the model predicts that the plateau region scales as $[\eta] \propto \phi^2$. The simulation data also shows some dispersion in the vicinity of plateau, however, much smaller than the theoretically predicted. Thus, the intrinsic viscosity provides a satisfactory scaling with respect to the concentration ϕ of the colloidal particles along the whole viscometric curve.